



Self-limiting CVD of a passivating SiO_x control layer on InGaAs(001)-(2x4) with the prevention of III-V oxidation



Mary Edmonds^a, Steven Wolf^a, Evgueni Chagarov^b, Tyler Kent^a, Jun Hong Park^a,
Russell Holmes^c, Daniel Alvarez^c, Ravi Droopad^d, Andrew C. Kummel^{a,b,*}

^a Materials Science and Engineering Program University of California, San Diego, La Jolla, CA 92093, United States

^b Department of Chemistry and Biochemistry University of California, San Diego, La Jolla, CA 92093, United States

^c Rasirc Inc., San Diego, CA 92126, United States

^d Ingram School of Engineering, Texas State University, San Marcos, TX 78666, United States

A B S T R A C T

A thin passivating SiO_x control layer has been deposited via self-limiting CVD on the InGaAs(001)-(2x4) surface by first depositing 2 monolayers of silicon with –Cl₂ termination using Si₂Cl₆, and then subsequently oxidizing the silicon seed layer by employing anhydrous HOOH(g) at a substrate temperature of 350 °C. After HOOH(g) dosing, XPS spectra show a higher binding energy shoulder peak on Si2p indicative of SiO_x bonding, while an unshifted Si 2p component remains, and In 3d, Ga 2p, and As 2p peaks show no higher binding energy components consistent with the prevention of III-V oxidation. Scanning tunneling spectroscopy (STS) measurements show after SiO_x deposition on the InGaAs(001)-(2x4) surface, the bandgap broadens towards that of SiO₂, with the electronic structure free of states in the bandgap leaving the surface ready for subsequent gate oxide ALD. Density functional theory calculations support the experimental STS data following TMA dosing, which shows TMA nucleates directly on the SiO_x/InGaAs(001) surface and leaves an electrically passive interface with the bandgap free of defect states and the surface ready for high-K gate oxide nucleation.

1. Introduction

InGaAs contains intrinsically high electron mobility, making it a promising candidate for replacement of silicon in the n-type channel region of metal oxide semiconductor field effect transistors (MOSFETs) [1–3]. One of the challenges of replacing silicon channels by III-V channels is the formation of a low defect, thermodynamically stable gate high-K dielectric which can match or exceed the capacitance and interfacial properties of HfO₂ on silicon. For process integration, it is critical that the high-k on III-V be amorphous and compatible with conventional back-end processing which makes integration of conventional amorphous high-k materials (such HfO₂ and ZrO₂) a priority. Previous reports show III-V suboxides and excess As₂O₅ and As₂O₃ pin the surface Fermi level, and InGaAs/GaAs native oxides serve as a poor dielectric gate as the oxides are unstable and leaky [4,5]. Deposition of high-K gate oxide directly on the GaAs(001) surface often produces poor capacitance-voltage characteristics such as large frequency dispersion, hysteresis, and high leakage current all of which are attributed to the formation of interfacial III-V oxides [6–8]. In this report, a thin saturating silicon oxide control layer is deposited by self-limiting reaction chemistry on the InGaAs(001) surface in order to eliminate

III-V dangling bonds by passivating with silicon, and to create a surface interfacial silicon layer terminated with –OH and –O groups which can nucleate high-K gate oxide ALD with virtually any metal precursor while protecting the III-V surface from oxidation.

Previous work has shown that deposition of a thin passivating MBE silicon control layer on In_{0.53}Ga_{0.47}As(100) prior to Al₂O₃ gate oxide deposition improved MOSFET performance by lowering frequency dispersion, reducing hysteresis, and lowering interfacial trap density (D_{it}) [9]. Similarly, physical vapor deposition (PVD) of a silicon control layer (1.5 nm) on GaAs(001) effectively passivated the III-V surface and protected against oxygen diffusion to the III-V surface as well as prevented formation of high D_{it} during high temperature annealing of MOS gate stacks [10,11]. These MBE and PVD methods improve the interfacial properties between the high-K gate oxide and III-V surface with nanometer scale films, but in order to continue scaling MOSFET size in a 3D topology such as a finFET and maintain an EOT below 1 nm, ALD and self-limiting CVD methods must be implemented for more precise deposition at the subnanometer range.

Silicon ALD on SiO₂ was reported with alternate pulses of Si₂H₆ and SiCl₄ at substrate temperatures of 355–385 °C, and each ALD cycle required several minutes as the HCl(g) desorption byproduct formation

* Corresponding author at: Materials Science and Engineering Program University of California, San Diego, La Jolla, CA 92093, United States

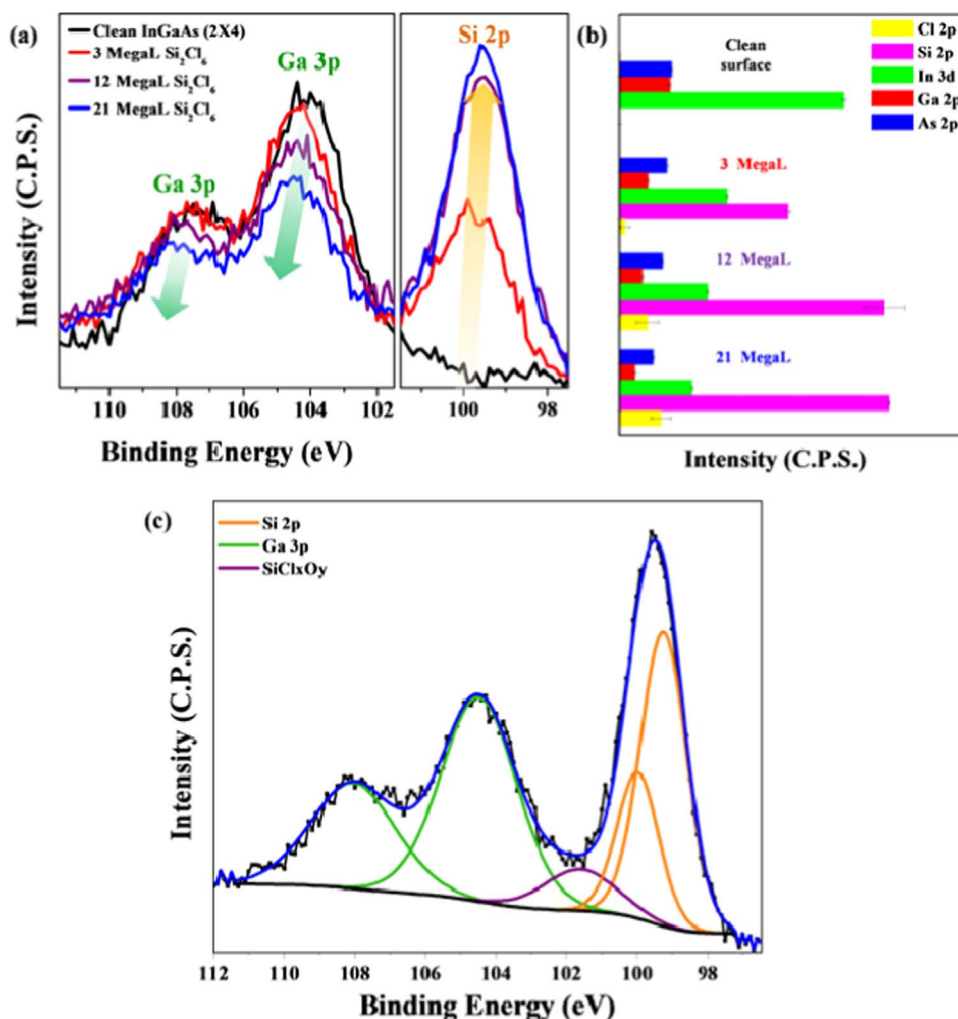


Fig. 1. XPS of Si₂Cl₆ on InGaAs(001)-(2x4). XPS raw counts corrected by Schofield photoionization cross sectional relative sensitivity factors. (a) Raw XPS peak areas for Ga 3p and Si 2p on clean InGaAs(2x4), and following 3, 12, and 21 MegaLangmuir total Si₂Cl₆ doses at 350 °C. (b) XPS corrected peak areas for 3 MegaLangmuir Si₂Cl₆, 12 MegaLangmuir Si₂Cl₆, and 21 MegaLangmuir Si₂Cl₆ on n-type InGaAs(001)-(2x4). All doses at 350 °C. (c) XPS peak fitting of Si 2p and Ga 3p peaks following 21 MegaLangmuir Si₂Cl₆. Ga 3p spin orbit split peaks are shown in green, SiCl_xO_y component shown in purple, and Si 2p spin orbit split peaks shown in orange. (For interpretation of the references to color in this figure legend, the reader is referred to the web version of this article.)

is slow below 400 °C [12]. Silicon ALD was reported on Ge substrates by alternating pulses of Si₂Cl₆ and atomic hydrogen, or SiH₂Cl₂ and SiH₄, at substrate temperatures of 400–560 °C [13,14]. Silicon ALD processes on Si substrates have been reported with alternating pulses of SiH₂Cl₂ and atomic hydrogen, or Si₂H₆ and Si₂Cl₆, at substrate temperatures (400–560 °C) [15,16]. These ALD processes employ high substrate temperatures which may desorb the passivating ligand and may cause changes in substrate reconstruction or composition for InGaAs and related III-V materials [17]. Previous work reported SiO₂ ALD by cyclically dosing ozone and tris(dimethylamino)silane at room temperature on Si(100), plasma assisted SiO₂ ALD by sequentially pulsing H₂Si[N(C₂H₅)₂]₂ and O₂ plasma at 50–400 °C on Si(100), and room temperature SiO₂ CVD on Si(100) by SiCl₄ and H₂O in the presence of a NH₃ catalyst [5–7]. SiO₂ ALD has been reported on GaAs(001) at room temperature by cyclically dosing SiCl₄ and H₂O in the presence of anhydrous pyridine [18]. The study reported the SiO₂ films lead to formation of higher oxidation states of both Ga and As and concurrently higher D_{it} which was only eliminated after high temperature post deposition annealing at 400–600 °C. The present study reports upon, a plasma-less self-limiting CVD process to deposit a thin Si-O_x control layer (9–10 Å) on the InGaAs(001)-(2x4) surface through dosing Si₂Cl₆ followed by anhydrous HOOH(g) at 350 °C with no post deposition annealing; the process prevents III-V substrate oxidation as

determined by XPS, while maintaining an unpinned surface Fermi level as shown by STS measurements, leaving the III-V surface passivated and ready for high-K gate oxide deposition.

2. Experimental details

This work employs n-type (Si dopant) samples consisting of 0.2 μm of 1–2x10¹⁸ doped In_{0.53}Ga_{0.47}As(001) layers grown by MBE on commercially available InP(001) substrates. The samples are capped with an As₂ layer (50 nm) and shipped/stored under vacuum prior to introduction into the Omicron ultrahigh vacuum (UHV) preparation chamber with a base pressure of 1x10⁻¹⁰ Torr. In the preparation chamber, the samples are degassed at 250 °C for 30 min, then decapped and annealed for one hour by radiatively heating at 360–370 °C to obtain the arsenic rich InGaAs(001)-(2x4) surface reconstruction.

Following annealing, the samples are characterized by an Omicron *in situ* monochromatic XPS using the aluminum Kα excitation source (hν=1486.7 eV) with spectra recorded at a glancing angle of 30° to enhance surface sensitivity. XPS raw counts are recorded using the XPS constant analyzer energy mode with a pass energy of 50 eV and line width of 0.1 eV. XPS peak shape analysis is conducted using CASA XPS v.2.3 with Shirley background subtraction. All XPS raw core level peaks

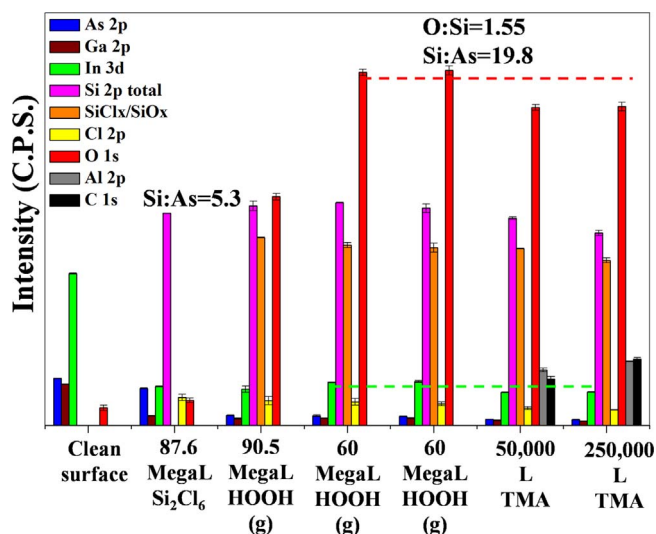


Fig. 2. XPS of Si_2Cl_6 , $\text{HOOH}(\text{g})$, and TMA on $\text{InGaAs}(001)-(2\times 4)$. XPS raw counts corrected by Schofield photoionization cross sectional relative sensitivity factors. XPS corrected peak areas of As 2p, Ga 2p, In 3d, Si 2p (total signal and higher binding energy shifted component), Cl 2p, O 1s, Al 2p, and C 1s of the decapped $\text{InGaAs}(001)-(2\times 4)$ surface, and following 87.6 MegaLangmuir Si_2Cl_6 , 90.5 MegaLangmuir $\text{HOOH}(\text{g})$, an additional 60 MegaLangmuir $\text{HOOH}(\text{g})$, a final 60 MegaLangmuir $\text{HOOH}(\text{g})$ exposure, 50,000 L TMA, and an additional 250,000 L TMA. All Si_2Cl_6 and $\text{HOOH}(\text{g})$ exposures at a substrate temperature of 350 °C, and TMA doses at a substrate temperature of 250 °C.

are corrected by Schofield photoionization cross sectional relative sensitivity factors. Following XPS elemental analysis, the samples are transferred to the SPM chamber (base pressure of 2×10^{-11} Torr), where scanning tunneling microscopy (STM) is performed at 300 K to determine the atomic order of the surface by using constant current mode with the tunneling current set point at 0.1 nA and the sample bias set to -3 V for filled state imaging. Scanning tunneling spectroscopy (STS) is performed to determine the electrical quality of the surface and probe the local surface density of states using variable- z mode with the sample bias swept from -1.5 to $+1.5$ V and the tip simultaneously moving towards and then away from the surface [19]. An applied Δz initial offset ranging from -0.2 to -0.8 nm is used to maximize $I(V)$ signal without crashing the STM tip. The dI/dV spectra are recorded using a lock-in amplifier and STS curves are reported by averaging 12 or more single curves taken across the sample surface. The curves are fitted (dashed red line in reported spectra) using a method described in previous STM/STS studies to extract the measured band edge energies of the collected (dI/dV) spectra [20–22]. The fits employ a linear function with slight rounding at the bandgap onset due to temperature and AC modulation. Standard errors are obtained by the fitting process and reported for the averaged STS curves. The uncertainties provided by the fitting method are statistical uncertainties using least squares fitting [23], and the reported uncertainties are much less than thermal broadening in STS measurements.

After the initial characterization, the samples are transferred back to the preparation chamber and radiatively heated to 350 °C for 15 min while simultaneously heating the high vacuum ALD chamber manipulator to 350 °C for 15 min to facilitate a faster sample transfer. All doses are performed in the high vacuum ALD chamber, and exposures are measured in Langmuirs (1×10^{-6} Torr/1 s) by a convectron gauge located in the HV-ALD chamber. The SiO_x deposition process is described as a self-limiting CVD process due to the initial InGaAs substrate surface induced etching by chlorine dissociated ligands from Si_2Cl_6 , keeping the process from classification as true ALD [24,25]. Previous work describes the self-limiting deposition of silicon on $\text{InGaAs}(001)-(2\times 4)$ [26], which includes the InGaAs substrate exposed to a saturation dose of Si_2Cl_6 at 350 °C.

In this work, the SiO_x self-limiting CVD process begins with an 87.6

MegaLangmuir total Si_2Cl_6 exposure at 350 °C (25 s pulses of 2.5×10^{-2} Torr) and post XPS analysis to confirm saturation of silicon with $-\text{Cl}$ termination on the $\text{InGaAs}(001)$ surface. Following saturation of Si-Cl_x on the $\text{InGaAs}(001)-(2\times 4)$ surface, the sample is subsequently exposed to anhydrous $\text{HOOH}(\text{g})$ at 350 °C to induce $\text{HOCl}(\text{g})$ and $\text{HCl}(\text{g})$ desorption and leave the silicon bonded to $-\text{OH}$ and $-\text{O}$ groups to create the self-limiting and saturating SiO_x control layer. The anhydrous $\text{HOOH}(\text{g})$ is delivered by Teflon tubing to the stainless steel HV-ALD chamber in order to minimize $\text{HOOH}(\text{g})$ decomposition. The anhydrous $\text{HOOH}(\text{g})$ is produced from a Teflon vessel which contains a membrane and a solvent based $\text{HOOH}(\text{g})$ solution (developed by Rasirc, Inc). The hydrogen peroxide diffuses across a largely gas-impermeable ionic exchange membrane within the vaporizer. The solvent cannot cross the membrane, which allows $\text{HOOH}(\text{g})$ to pass through to the HV-ALD chamber while preventing passage of the solvent, making the delivered dose anhydrous $\text{HOOH}(\text{g})$. The exposures are reported in Langmuirs assuming a 0% dissociation rate of $\text{HOOH}(\text{g})$. The sample is introduced to three total anhydrous $\text{HOOH}(\text{g})$ exposures at 350 °C: 90.5 MegaLangmuir $\text{HOOH}(\text{g})$, followed by two additional 60 MegaLangmuir $\text{HOOH}(\text{g})$ exposures, where each exposure consists of 45 s pulses of 5×10^{-2} Torr. Following each $\text{HOOH}(\text{g})$ dose, the sample is transferred back to the preparation chamber where XPS is performed. Following $\text{HOOH}(\text{g})$ dosing, the sample is heated to 250 °C and trimethylaluminum (TMA) is introduced by dosing 50,000 L and an additional 250,000 L; TMA is dosed with 5 milli Torr continuous pulses for 10 s and 5 s.

3. DFT computational details

The Density-Functional Theory (DFT) simulations are performed using the VASP plane-wave DFT simulation package with PBE exchange-correlation functional and projector augmented-wave (PAW) pseudopotentials [27–33]. The InGaAs slab is simulated as a regular polymorph with equal number of Ga and In atoms. Initially, the InGaAs unit cell is optimized at a variable volume to avoid internal compression/strain. This DFT-optimized unit cell is subsequently employed to build the InGaAs supercell and initial slabs with the desired surface terminations. All slab relaxations are performed using a conjugate-gradient (CG) relaxation algorithm with a force tolerance level of 0.05 eV/Å and Gamma-centered $5\times 7\times 1$ K-point grid. During the relaxations the 3 bottom layers of the InGaAs slabs are permanently fixed in their bulk-like positions and saturated with pseudo-H atoms with a 1.25 $|e|$ charge to simulate a continuous bulk. The atoms at the upper surface layers are passivated by normal 1.0 $|e|$ H atoms. To avoid a possible dipole effect, dipole correction in vertical Z direction was applied.

4. Results and discussion

Fig. 1(a) shows the raw XPS peak areas for Ga 3p and Si 2p peaks on the clean (2×4) surface, and following 3, 12, and 21 MegaLangmuir Si_2Cl_6 doses at 350 °C. The Ga 3p spin orbit split peaks are located at binding energies 104.4 eV and 108.2 eV, the Si 2p spin orbit split peaks are located at binding energy 99.8 eV. The Si 2p 1/2 and 3/2 spin orbit split peaks are resolved for 12 and 21 MegaLangmuir Si_2Cl_6 total doses and each additional dose increases the Si 2p peak area and decreases the substrate Ga 3p peak areas, indicative of increasingly higher silicon coverage until surface saturation is reached and the surface silicon left terminated by chlorine.

Fig. 1(b) shows the surface elemental composition from XPS for the clean n-type $\text{InGaAs}(001)-(2\times 4)$ surface, and following 3, 12, and 21 MegaLangmuir Si_2Cl_6 doses. In 3d, Ga 2p, and As 2p higher binding energy peaks are chosen in order to analyze the top most monolayers of the surface. 21 MegaLangmuir Si_2Cl_6 is 7 times the initial 3 MegaLangmuir dose, yet the increase in Si 2p corrected peak area is only $1.87\times$. The XPS data is consistent with a self-limiting CVD growth

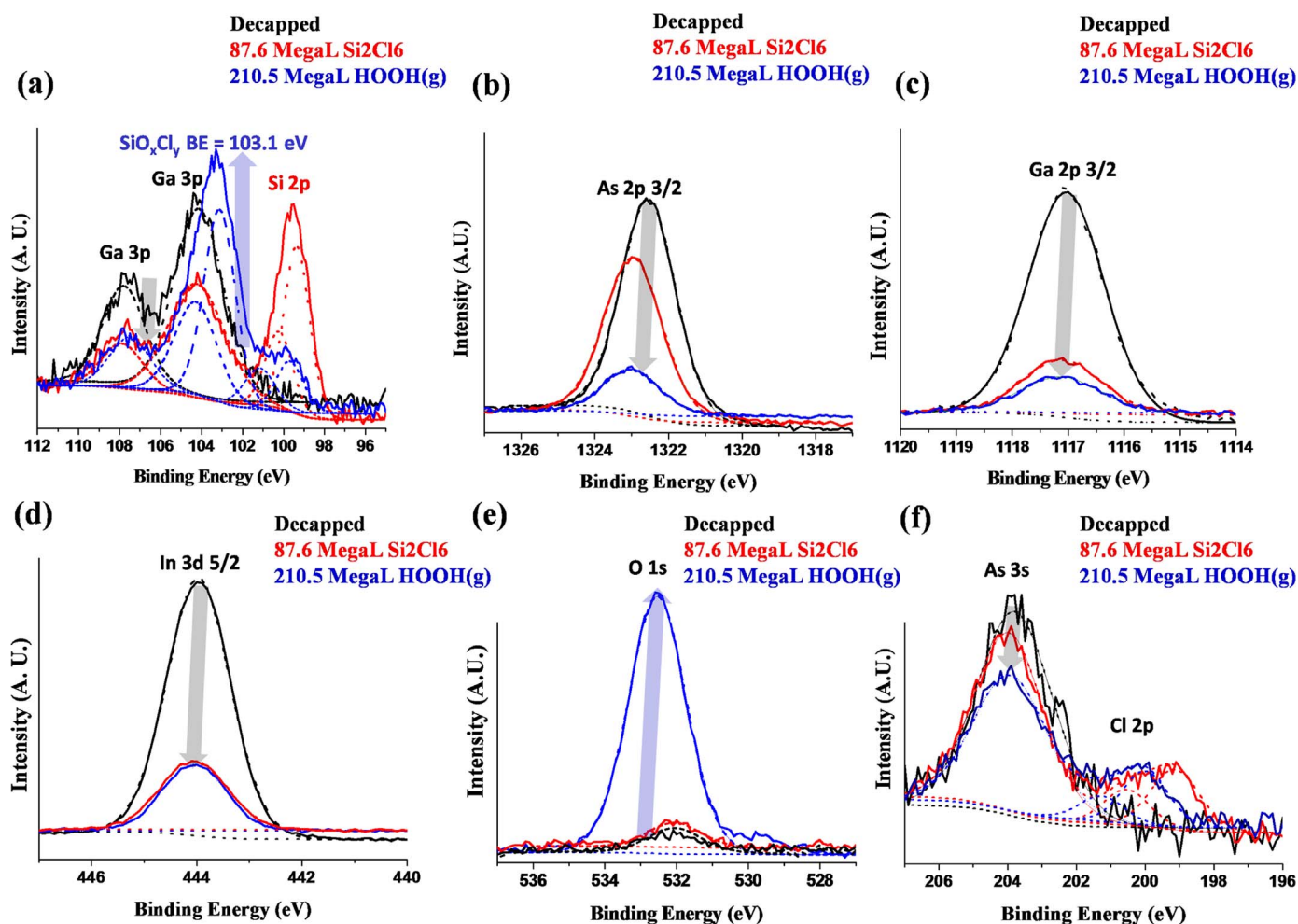


Fig. 3. XPS spectra after Si_2Cl_6 and $\text{HOOH}(\text{g})$ exposure on $\text{InGaAs}(001)-(2\times 4)$. XPS raw peak areas of Si 2p (a), As 2p 3/2 (b), Ga 2p 3/2 (c), In 3d 5/2 (d), O 1s (e), and Cl 2p (f) on the decapped $\text{InGaAs}(001)-(2\times 4)$ surface, and following 87.6 MegaLangmuir Si_2Cl_6 , and 210.5 MegaLangmuir $\text{HOOH}(\text{g})$ total exposure. All doses performed at a substrate temperature of 350 °C. Black arrows show the attenuation of the substrate peaks, and blue arrows highlight the growth of the SiO_xCl_x and O 1s peaks following $\text{HOOH}(\text{g})$ dosing. (For interpretation of the references to color in this figure legend, the reader is referred to the web version of this article.)

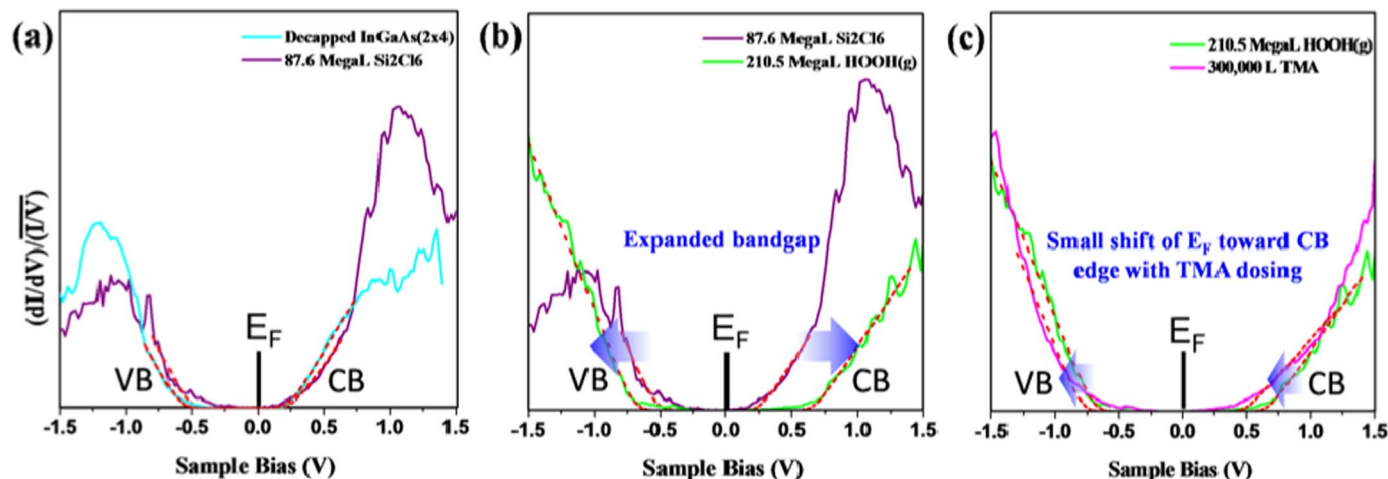


Fig. 4. STS of Si_2Cl_6 , $\text{HOOH}(\text{g})$, and TMA exposure on $\text{InGaAs}(001)-(2\times 4)$. (a) STS measurements on clean n-type $\text{InGaAs}(2\times 4)$ (teal curve), and following 87.6 MegaLangmuir Si_2Cl_6 at 350 °C (purple curve). (b) STS of clean n-type $\text{InGaAs}(2\times 4)$ dosed with 87.6 MegaLangmuir Si_2Cl_6 , and an additional 210.5 MegaLangmuir $\text{HOOH}(\text{g})$ at 350 °C (green curve). (c) STS of clean n-type $\text{InGaAs}(2\times 4)$ dosed with 87.6 MegaLangmuir Si_2Cl_6 and 210.5 MegaLangmuir $\text{HOOH}(\text{g})$ at 350 °C (green curve), and an additional 300,000 L TMA dosed at 250 °C (pink curve). Blue arrows indicate the shifting direction of the conduction band and valence band edges after $\text{HOOH}(\text{g})$ and TMA doses. (For interpretation of the references to color in this figure legend, the reader is referred to the web version of this article.)

process. Fig. 1(b) shows the chlorine signal is negligible following the initial 3 MegaLangmuir Si_2Cl_6 dose but is more prominent following the 12 and 21 MegaLangmuir doses consistent with excess surface

gallium and indium initially being preferentially etched by chlorine [25]. Once excess surface gallium and indium species have been etched and all clean In, Ga, and As surface sites have reacted with Si-Cl_x , the

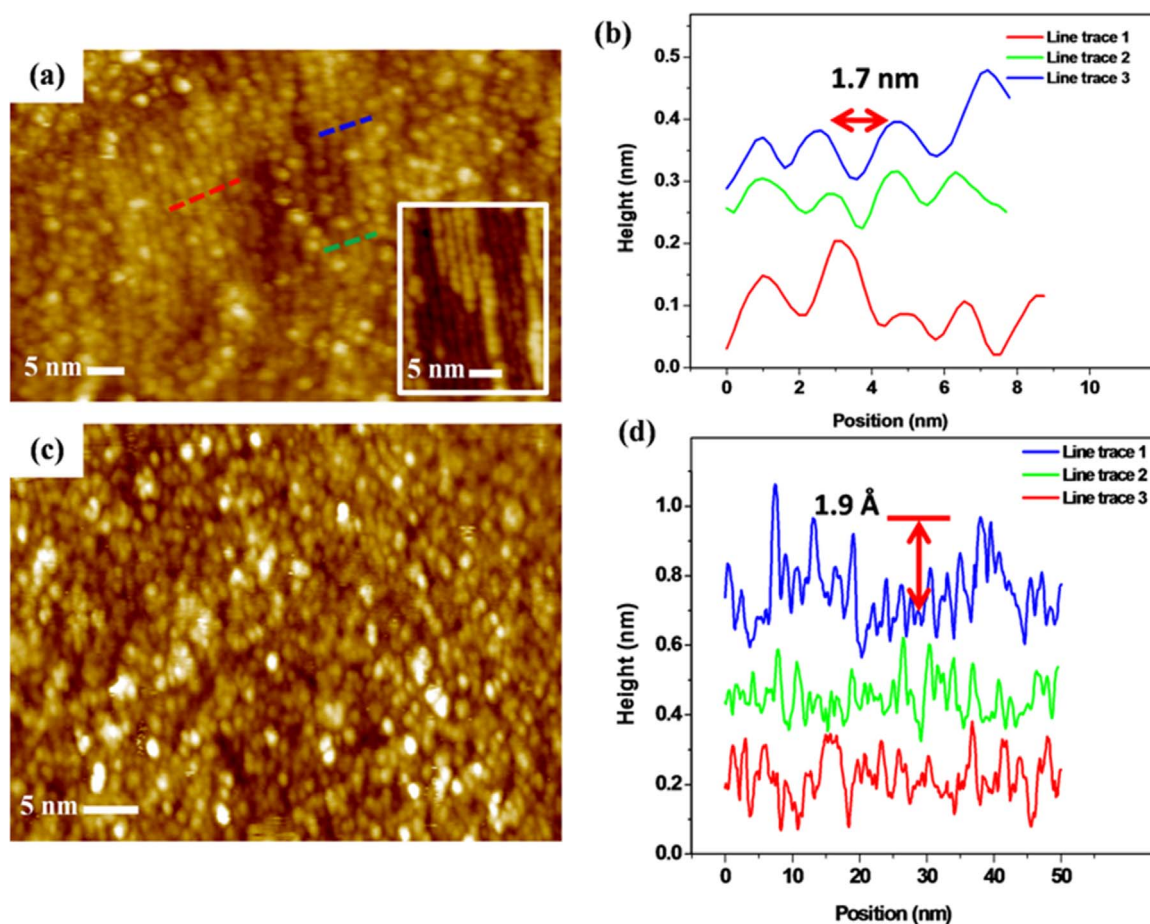


Fig. 5. STM of Si_2Cl_6 , and $\text{HOOH}(\text{g})$ saturation on $\text{InGaAs}(001)-(2\times 4)$. (a) Filled state STM image of 87.6 MegaLangmuir Si_2Cl_6 dosed at 350 °C on the $\text{InGaAs}(001)-(2\times 4)$ surface. The left-hand lower corner contains an enlarged inset of the clean $\text{InGaAs}(001)-(2\times 4)$ surface. (b) Line traces taken across the STM image shown in (a) along the ordered row regions seen across the surface following 87.6 MegaLangmuir Si_2Cl_6 . Row spacing is measured at 1.7 ± 0.07 nm. (c) Filled state STM image of 87.6 MegaLangmuir Si_2Cl_6 dosed at 350 °C followed by an additional 210.5 MegaLangmuir $\text{HOOH}(\text{g})$ at 350 °C on the $\text{InGaAs}(001)-(2\times 4)$ surface. (d) Line traces taken across the STM image shown in (c) indicating the surface features vary in height by no more than $\sim 1.9 \pm 0.2$ Å showing the surface contains high uniform coverage of SiO_x .

surface becomes saturated by chlorine termination as shown following the total 12, and 21 MegaLangmuir Si_2Cl_6 doses as chlorine desorption from silicon is close to zero at 350 °C [26,34]. Fig. 1(c) shows the deconvolution of Ga 3p 1/2 and 3/2 spin orbit split peaks, Si 2p 1/2 and 3/2 spin orbit split peaks, and the higher binding energy SiCl_xO_y component following the saturation dose of 21 MegaLangmuir Si_2Cl_6 . The higher binding energy component located at 100.5–101 eV is indicative of Si-Cl_x/Si-O_x bonding with oxygen presence consistent with a small amount of oxygen contamination over the course of the experiment [see Supplemental material] [35,36]. The SiCl_xO_y component makes up ~11% of the total Si 2p signal, showing that the majority of silicon deposited on the surface is unshifted Si^{+0} .

For the $\text{HOOH}(\text{g})$ functionalization, the $\text{InGaAs}(001)-(2\times 4)$ surface is initially exposed to 87.6 MegaLangmuir Si_2Cl_6 at 350 °C, and XPS results confirm 2 monolayers of silicon coverage with chlorine termination (Fig. 2). Following the Si-Cl_x saturation, anhydrous $\text{HOOH}(\text{g})$ is dosed on the surface to induce desorption of $\text{HCl}(\text{g})$ and $\text{HOCl}(\text{g})$ by-products, and leave the surface terminated by -O and -OH groups. Fig. 2 shows the XPS corrected peak areas of As 2p, Ga 2p, In 3d, Si 2p (total signal and higher binding energy shifted component), Cl 2p, O 1s, Al 2p, and C 1s of the decapped $\text{InGaAs}(001)-(2\times 4)$ surface, and following 87.6 MegaLangmuir Si_2Cl_6 , 90.5 MegaLangmuir $\text{HOOH}(\text{g})$, an additional 60 MegaLangmuir $\text{HOOH}(\text{g})$, and a final 60 MegaLangmuir $\text{HOOH}(\text{g})$ exposure with all doses at a substrate temperature of 350 °C. After a total of 150.5 MegaLangmuir $\text{HOOH}(\text{g})$, the -O coverage on the surface saturates as there is no further increase in the oxygen signal even after dosing an additional 60

MegaLangmuir (210.5 MegaLangmuir $\text{HOOH}(\text{g})$ total). It is hypothesized that some chlorine may be bound to silicon subsurface, and serves to block oxygen from fully oxidizing the silicon bilayer to SiO_2 , as the ratio of oxygen to silicon is ~1.55, and there is still unshifted silicon, and residual chlorine following $\text{HOOH}(\text{g})$ dosing.

Following the saturation $\text{HOOH}(\text{g})$ dosing, the surface is exposed to TMA in order to determine if a high-K metal ALD precursor would directly nucleate on the surface. TMA is dosed at a sample temperature of 250 °C, with an initial 50,000 L exposure followed by an additional 250,000 L. The aluminum and carbon signals observed in XPS (Fig. 2) are consistent with dimethylaluminum groups being present on the surface. The TMA coverage on the surface is found to saturate as 250,000 L is 5 times the initial TMA exposure, but the change in coverage of aluminum is only 1.2× and the change in carbon is 1.5×.

The thickness of the deposited SiO_x layer was calculated based upon the equation reported by D. F. Mitchell et. al: $\lambda \sin(\theta) \ln(I/I_0) = -t$, where (I/I_0) is the intensity of the substrate signal before and after depositing a film of thickness t , λ is the inelastic mean free path of the collected electrons, and θ is the take-off angle of the collected electrons with respect to the surface parallel [37,38]. The SiO_x film thickness was calculated from the above equation and the experimental ratio of Si2p/As2p following saturation Si_2Cl_6 and $\text{HOOH}(\text{g})$ doses. In this model, t is the thickness of the deposited SiO_x layer, θ is the take-off angle of collected electrons (30° with respect to parallel), and λ is the inelastic mean free path of the collected electrons from the As 2p 3/2 core shell (0.699 nm) and the Si 2p core shells (2.1 nm) [37,38]. The As 2p peak was chosen for the thickness calculation because the silicon deposition

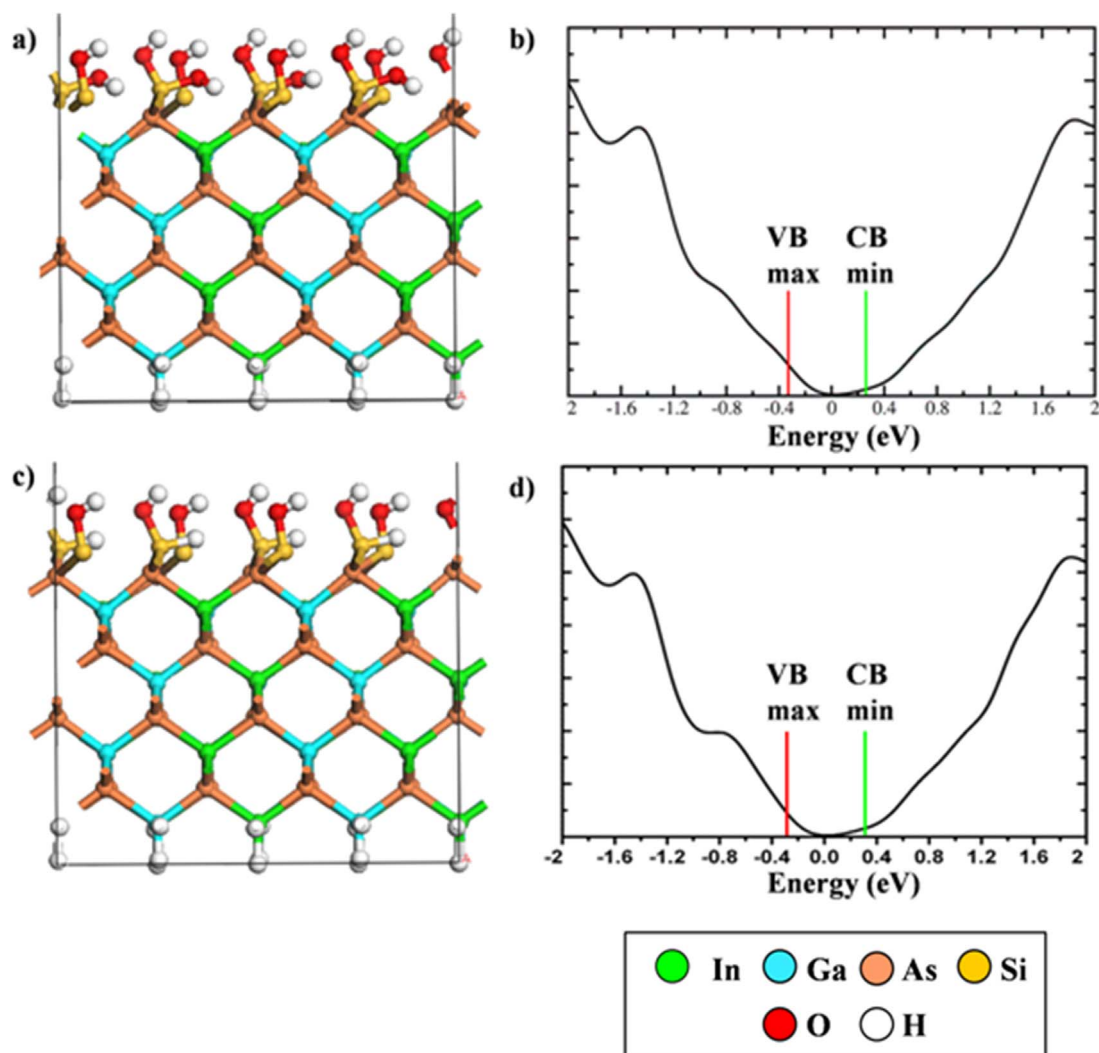


Fig. 6. DFT simulations of SiO_x passivation on InGaAs(001). (a) As-rich InGaAs(001) unit cell with half the surface As bonded to one Si-OH group (with one filled dangling bond on Si), and half the surface As bonded to one Si bonded to two -OH groups. (b) calculated DOS for the model shown in (a) containing a narrow bandgap. (c) As-rich InGaAs(001) surface with each surface As bonding to one Si-OH group (with one filled dangling bond on Si), and one Si bonded to an H atom, and an -OH group. (d) calculated DOS for the model presented in (c) containing a narrow bandgap. Valence band maximum and conduction band minimum values are marked by red and green lines. (For interpretation of the references to color in this figure legend, the reader is referred to the web version of this article.)

process led to preferential etching of surface indium and gallium species. The model used uniform slabs of 0.05 nm thickness assuming the SiO_x has $x=1.55$ (as shown by the XPS data in Fig. 2) and the substrate was 50% As. To match the experimental Si 2p/As 2p ratio of 19.8 (from XPS data in Fig. 2), the SiO_x layer is ~ 0.93 nm thick. To confirm the results, the thickness of the Si layer after saturation Si_2Cl_6 dosing was estimated from the experimentally observed Si 2p/As 2p ratio of 5.3 (See Fig. 2); again assuming the substrate is 50% As while the silicon layer is 100% Si, the thickness is estimated as 0.38 nm. This 0.38 nm of pure Si corresponds with the estimate 0.93 nm of $\text{SiO}_{1.55}$ after saturation $\text{HOOH}(\text{g})$ showing the estimates are self consistent.

Fig. 3 shows the XPS raw peak areas for Si 2p, As 2p 3/2, Ga 2p 3/2, In 3d 5/2, O 1s, and Cl 2p on the decapped InGaAs(001)-(2x4) surface, and following 87.6 MegaLangmuir Si_2Cl_6 at 350 °C, and 210.5 MegaLangmuir total $\text{HOOH}(\text{g})$ at 350 °C. The Si 2p peak (Fig. 3(a)) after the Si_2Cl_6 dose is found at binding energy 99.8 eV, and following the $\text{HOOH}(\text{g})$ exposure the peak shifts to 103.1 eV, which is within the binding energy range reported for substoichiometric SiO_x films in the literature [39]. A small unshifted Si 2p peak remains at 99.8 eV showing the $\text{HOOH}(\text{g})$ is unable to fully oxidize the Si control layer, as residual chlorine may serve to prevent full oxidation of silicon to the +4 state and may also protect silicon back-bonds to the substrate from

being oxidized.

Fig. 3(b) shows the As 2p 3/2 peak undergoes a chemical shift to higher energy of ~ 0.5 eV consistent with formation of As-Si bonds, but no higher binding energy shoulder components are observed on the In, Ga, or As substrate peaks (Fig. 3(b)–(d)), indicating no oxidation of the substrate has occurred. The As 3d core level XPS peaks before and after Si_2Cl_6 dosing are shown in the supplement demonstrating the same core level shift of ~ 0.5 eV in higher binding energy. On the clean surface, there are As-As bonds and As dangling bonds. While substitution of As-As bonds for As-Si should have little effect on the As peak energy, substitution of As dangling bonds for As-Si covalent bonds should increase the As peak energy [40]. Any etching of In or Ga which results in substitution of As-In or As-Ga bonds for As-Si will also contribute to the increase in As electron binding energy. Fig. 3(f) shows chlorine still remains on the surface following the $\text{HOOH}(\text{g})$ exposure.

Fig. 4(a) shows the STS measurements probing the local surface density of states of the n-type decapped InGaAs(001)-(2x4) surface before (teal curve) and after saturation Si_2Cl_6 dosing (purple curve) at 350 °C. Following 87.6 MegaLangmuir Si_2Cl_6 , the conduction and valence band edges align with the clean (2x4) surface, the Fermi level position lies near the conduction band edge, and there are no defect states observed inside the bandgap indicating the surface Fermi level

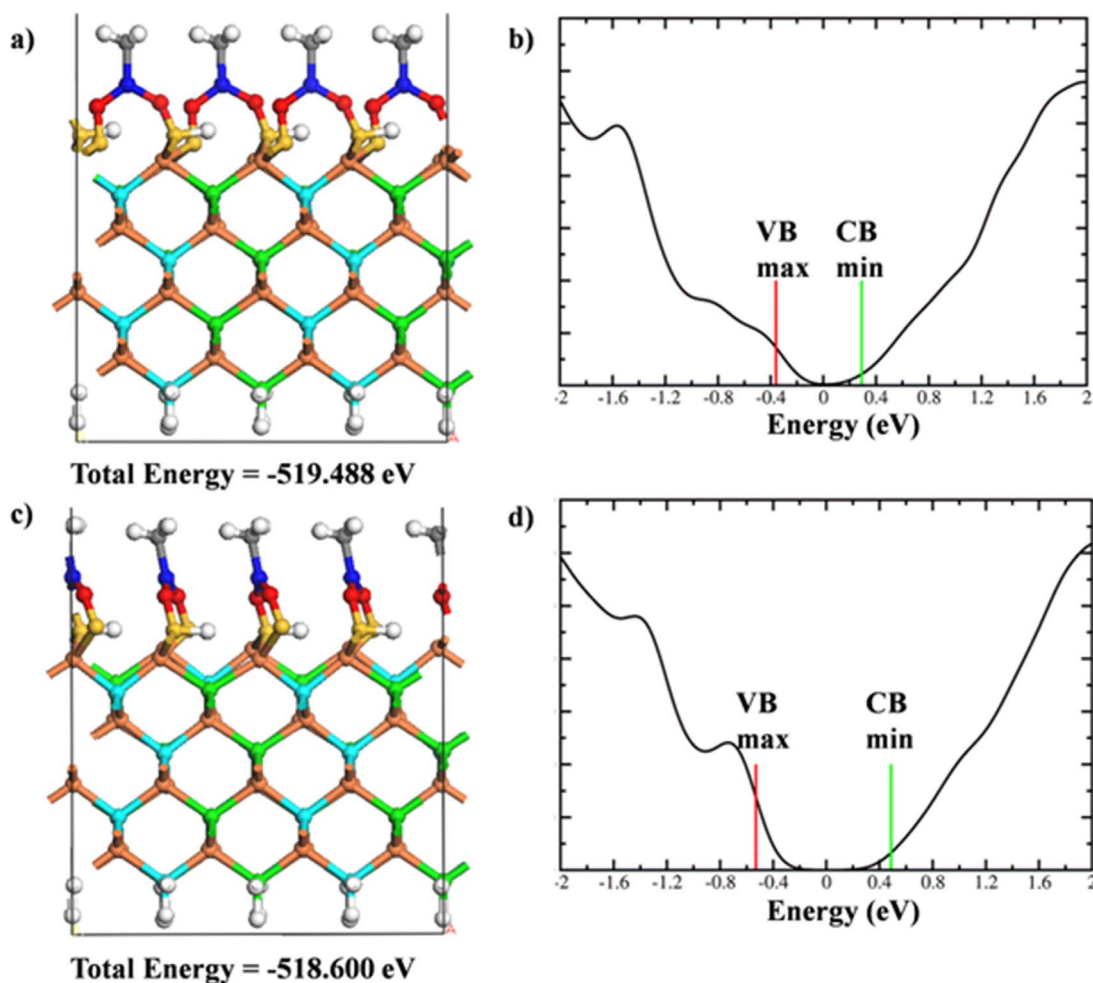


Fig. 7. DFT simulations of TMA on SiO_x/InGaAs(001). (a) As rich InGaAs(001) unit cell with SiO_x configuration shown in Fig. 6(c) with monomethyl-aluminum (MMA) groups bridge bonding between neighboring oxygen atoms. (b) calculated DOS for the model shown in (a) containing a narrow bandgap. (c) As rich InGaAs(001) unit cell with SiO_x configuration shown in Fig. 6(c) with MMA groups bridge bonding between adjacent, closer neighboring oxygen atoms. (d) calculated DOS for the models shown in (c) with a large bandgap. Valence band maximum and conduction band minimum values are marked by red and green lines. Total energies are shown below each model. (For interpretation of the references to color in this figure legend, the reader is referred to the web version of this article.)

remains unpinned.

Fig. 4(b) shows an overlay of STS measurements following 87.6 MegaLangmuir Si₂Cl₆ (purple curve), and following 210.5 MegaLangmuir HOOH(g) at 350 °C (green curve). After HOOH(g) dosing, the surface Fermi level is shifted to midgap (shown by blue arrows) consistent with surface dipole formation from –OH groups and oxygen bonding to the surface. The bandgap increases from $\sim 0.78 \pm 0.02$ eV to $\sim 1.37 \pm 0.02$ eV as the surface is now terminated by 0.93 nm of SiO_x. Modest bandgaps, ranging from 1.5 eV to 3 eV, for thin SiO_x films with $x < 2$ have been reported in literature [41–43].

Fig. 4(c) shows the STS measurements after 87.6 MegaLangmuir Si₂Cl₆ and 210.5 MegaLangmuir HOOH(g) at 350 °C (green curve), and an additional 300,000 L TMA dosed at 250 °C (pink curve). After TMA dosing, the bandgap (1.27 ± 0.02 eV) is nearly the same size as that after HOOH(g) dosing, and the Fermi level position is shifted slightly above midgap closer to the conduction band edge (shown by blue arrows), consistent with surface Fermi level unpinning and the –OH and –O induced surface dipole being lessened through surface bonding with dimethylaluminum groups.

Fig. 5(a) shows a filled state STM image of the clean n-type InGaAs(001)-(2x4) surface following 87.6 MegaLangmuir Si₂Cl₆ dosed at 350 °C with an inset in the lower left-hand corner showing the clean InGaAs(2x4) surface. Fig. 5(b) shows a typical line trace taken across the ordered row region of the STM image shown in (a) after saturation Si₂Cl₆ dosing. The clean (2x4) surface contains surface terminating As-

As dimer rows spaced at ~ 1.7 nm, and after Si₂Cl₆ dosing the surface remains quasi-ordered with ordered rows seen along the same direction as the underlying (2x4) surface rows at an average row spacing of 1.7 ± 0.07 nm indicative of Si-Cl_x species absorbing in commensurate fashion with the underlying III-V substrate.

Fig. 5(c) shows the (2x4) surface following the saturated 87.6 MegaLangmuir Si₂Cl₆ dose at 350 °C, and a 210.5 MegaLangmuir HOOH(g) dose at 350 °C. The surface does not contain atomic ordering, but uniform SiO_x coverage is observed across the surface, as shown in Fig. 5(d), where line traces across the surface. Surface features are found to vary in height by less than one atomic step ($\sim 1.9 \pm 0.2$ Å) on the saturated SiO_x/InGaAs(001)-(2x4) surface showing high uniform nucleation and growth of SiO_x across the surface.

5. Density functional theory simulations

Initial DFT modeling of the SiO_x/InGaAs(001) interface with and without TMA passivation is performed in order to examine various interfacial bonding configurations. To model the InGaAs(001) surface bonding with silicon after dosing with Si₂Cl₆, the InGaAs surface is terminated by all sp [3] hybridized arsenic atoms. This arsenic-rich surface termination is consistent with the self-limiting and saturating Si₂Cl₆ deposition process: as shown by XPS, with higher coverage of Si₂Cl₆, the InGaAs surface becomes more arsenic-rich as surface In/Ga

species are preferentially etched by chlorine. Fig. 6(a) shows a model of the silicon passivated InGaAs(001) surface after dosing with HOOH(g): the Si capped As-rich InGaAs(001) surface is terminated with 50% Si-OH groups (with one filled dangling bond on Si), and 50% Si bonded to two -OH groups since this is the maximum -OH coverage which is consistent with the electron counting rule developed by M.D. Pashley for an unpinned charge neutral interface [44]. All DFT models shown in Figs. 6 and 7 follow the electron counting rule. The calculated density of states (DOS) for the bonding configuration shown in Fig. 6(a) shows a narrow bandgap with the Fermi level position located slightly above midgap (Fig. 6(b)). The narrow bandgap is consistent with Fermi level pinning. Fig. 6(c) shows the arsenic-rich InGaAs(001) surface with each surface arsenic bonding to one Si-OH group (with one filled dangling bond on Si), and one Si bonded to an H atom, and an -OH group. This model contains 2/3 the amount of -OH groups on the surface in order to assist in alleviating any steric hindrance from bulky -OH groups that can cause defect states in the band gap. The calculated DOS still shows a narrow bandgap consistent with Fermi level pinning, and the Fermi level position is located slightly above midgap.

Fig. 7 shows two different bonding configurations for monomethylaluminum (MMA) groups replacing hydrogen atoms bonding to all O atoms found in the Fig. 6(c) model. Fig. 7(a) shows MMA groups bridge bonding between neighboring oxygen atoms. Fig. 7(b) contains the calculated DOS which shows the Fermi level located slightly above midgap, and a narrow bandgap. Fig. 7(c) shows MMA groups bridge bonding between adjacent, closer neighboring oxygen atoms and the calculated DOS (Fig. 7(d)) contains a larger bandgap which is more reflective of experimental STS measurements confirming TMA passivation of the SiO_x/InGaAs(001) surface can produce an electrically passive interface ready for high-K gate oxide deposition. The calculated total energies of the models in Fig. 7(a) and (c) are shown below each model in order to compare the relative thermodynamic stabilities of both passivation bonding configurations, as both models contain the same number of atoms. Fig. 7(a) contains ~0.9 eV lower total energy than the model shown in Fig. 7(c), indicating Fig. 7(a) is the slightly more energetically favorable bonding configuration, although Fig. 7(c) more closely reflects experimental STS measurements. A mixture of different surface bonding configurations is likely to be present within the deposited substoichiometric SiO_x film.

6. Conclusions

A thin SiO_x control layer (~0.9-1nm) is deposited on the InGaAs(001)-(2x4) surface by a plasma-less self-limiting CVD process by dosing Si₂Cl₆ followed by anhydrous HOOH(g) at 350 °C with no post deposition annealing required. High-k gate oxide, such as Al₂O₃, directly nucleates and saturates on the SiO_x terminated surface as confirmed with XPS measurements after dosing TMA at 250 °C. STM measurements show the self-limiting CVD process on InGaAs(001)-(2x4) produces a uniform SiO_x coverage as the surface features are found to vary in height by less than one atomic step. STS measurements show TMA dosing on the SiO_x/InGaAs surface leaves a bandgap free of midgap defect states with the Fermi level position found slightly above midgap closer to the conduction band edge, consistent with surface Fermi level unpinning and the -OH and -O induced surface dipole being lessened through surface bonding with MMA or DMA groups. DFT simulations of SiO_x passivation on InGaAs(001) show a narrow pinned bandgap consistent with experimental STS showing a surface induced dipole from -OH/O groups shifting the Fermi level midgap. DFT simulations indicate TMA passivation can lead to a bandgap free of defect states and surface Fermi level unpinning. XPS

shows this SiO_x growth process prevents III-V substrate oxidation, and maintains an unpinned surface Fermi level as shown by STS measurements and supported by DFT simulations, leaving the III-V surface passivated and ready for high-K gate oxide deposition.

Appendix A. Supporting information

Supplementary data associated with this article can be found in the online version at doi:10.1016/j.susc.2017.02.006.

References

- [1] R. Chau, In nanotechnology, 2004, in: Proceedings of the 4th IEEE Conference, IEEE, p. 3, 2004.
- [2] S. Datta, R. Chau, In indium phosphide and related materials, 2005, in: Proceedings of International Conference, IEEE, p. 7, 2005.
- [3] J.A. Del Alamo, Nature 479 (2011) 317.
- [4] C. Hinkle, M. Milojevic, B. Brennan, A. Sonnet, F. Aguirre-Tostado, G. Hughes, E. Vogel, R. Wallace, Appl. Phys. Lett. 94 (2009) 162101.
- [5] P.D. Ye, Birck and CN Publications, 2008, p. 134.
- [6] G. Dalapati, A. Sridhara, A. Wong, C. Chia, D. Chi, Appl. Phys. Lett. (2009) 94.
- [7] G.K. Dalapati, A. Sridhara, A.S.W. Wong, C.K. Chia, C. Dongzhi, S.J. Lee, J. Appl. Phys. (2008) 103.
- [8] D.C. Suh, Y.D. Cho, S.W. Kim, D.-H. Ko, Y. Lee, M.-H. Cho, J. Oh, Appl. Phys. Lett. 96 (2010) 2112.
- [9] M. Akazawa, H. Hasegawa, Appl. Surf. Sci. 256 (2010) 5708.
- [10] M.H. Zhang, M. Oye, B. Cobb, F. Zhu, H.S. Kim, I.J. Ok, J. Hurst, S. Lewis, A. Holmes, J.C. Lee, S. Koveshnikov, W. Tsai, M. Yakimov, V. Torkanov, S. Oktyabrsky, J. Appl. Phys. (2007) 101.
- [11] C. Marchiori, D. Webb, C. Rossel, M. Richter, M. Sousa, C. Gerl, R. Germann, C. Andersson, J. Fompeyrine, J. Appl. Phys. 106 (2009) 114112.
- [12] S. Yokoyama, K. Ohba, A. Nakajima, Appl. Phys. Lett. 79 (2001) 617.
- [13] D. Koleske, S. Gates, Appl. Phys. Lett. 64 (1994) 884.
- [14] K. Ikeda, S. Sugahara, Y. Uchida, T. Nagai, M. Matsumura, Japanese Journal of Applied Physics, vol. 37, 1998, p. 1311.
- [15] D. Koleske, S. Gates, D. Beach, J. Appl. Phys. 72 (1992) 4073.
- [16] E. Hasunuma, S. Sugahara, S. Hoshino, S. Imai, K. Ikeda, M. Matsumura, J. Vacuum Sci. Technol. A: Vacuum, Surf. Films 16 (1998) 679.
- [17] W. Melitz, J. Shen, T. Kent, A.C. Kummel, R. Droopad, J. Appl. Phys. 110 (2011) 013713.
- [18] G. Dalapati, C. Chia, C. Mahata, T. Das, C. Maiti, M. Kumar, H. Gao, S. Chiam, C. Tan, C. Chua, Electrochem. Solid-State Lett. 14 (2011) G52.
- [19] P. Mårtensson, R. Feenstra, Phys. Rev. B 39 (1989) 7744.
- [20] R.M. Feenstra, Phys. Rev. B 50 (1994) 4561.
- [21] R.M. Feenstra, J.Y. Lee, M.H. Kang, G. Meyer, K.H. Rieder, Phys. Rev. B (2006) 73.
- [22] R.M. Feenstra, J. Lee, M. Kang, G. Meyer, K. Rieder, Phys. Rev. B 73 (2006) 035310.
- [23] P.R. Bevington, D.K. Robinson, Data Reduction and Error Analysis for the Physical Sciences, 3rd ed, McGraw-Hill, Boston, 2003.
- [24] J.R. Creighton, J. Vacuum Sci. Technol. A 8 (1990) 3984.
- [25] S. Mokler, P. Watson, L. Ungier, J. Arthur, J. Vacuum Sci. Technol. B 10 (1992) 2371.
- [26] M. Edmonds, T. Kent, E. Chagarov, K. Sardashti, R. Droopad, M. Chang, J. Kachian, J.H. Park, A. Kummel, J. Am. Chem. Soc. 137 (2015) 8526.
- [27] P.E. Blöchl, Phys. Rev. B 50 (1994) 17953.
- [28] G. Kresse, J. Furthmüller, Comput. Mater. Sci. 6 (1996) 15.
- [29] G. Kresse, J. Furthmüller, Phys. Rev. B 54 (1996) 11169.
- [30] G. Kresse, J. Hafner, Phys. Rev. B 47 (1993) 558.
- [31] G. Kresse, J. Hafner, Phys. Rev. B 49 (1994) 14251.
- [32] G. Kresse, D. Joubert, Phys. Rev. B 1999 (1758) 59.
- [33] J.P. Perdew, K. Burke, M. Ernzerhof, Phys. Rev. Lett. 77 (1996) 3865.
- [34] Q. Gao, Z. Dohnalek, C. Cheng, W. Choyke, J. Yates Jr., Surf. Sci. 302 (1994) 1.
- [35] M. El Kazzi, L. Czornomaz, D. Webb, C. Rossel, D. Caimi, H. Siegwart, J. Fompeyrine, C. Marchiori, Appl. Phys. Lett. 99 (2011) 052102.
- [36] E.J. Nemanick, P.T. Hurley, L.J. Webb, D.W. Knapp, D.J. Michalak, B.S. Brunshwig, N.S. Lewis, J. Phys. Chem. B 110 (2006) 14770.
- [37] D. Mitchell, K. Clark, J. Bardwell, W. Lennard, G. Massoumi, I. Mitchell, Surf. Interface Anal. 21 (1994) 44.
- [38] M. Seah, W. Dench, Surf. Interface Anal. 1 (1979) 2.
- [39] R. Alfonsetti, L. Lozzi, M. Passacantando, P. Picozzi, S. Santucci, Appl. Surf. Sci. 70 (1993) 222.
- [40] H. Hasegawa, M. Akazawa, H. Ishii, A. Uraie, H. Iwadata, E. Ohue, J. Vacuum Sci. Technol. B: Microelectron. Process. Phenom. 8 (1990) 867.
- [41] H. Philipp, J. Phys. Chem. Solids 1971 (1935) 32.
- [42] A. Shabalov, M. Feldman, Thin Solid Films 151 (1987) 317.
- [43] H. Watanabe, T. Baba, M. Ichikawa, J. Appl. Phys. 85 (1999) 6704.
- [44] M. Pashley, Phys. Rev. B 40 (1989) 10481.